ARMY RESEARCH LABORATORY

Computational Fluid Dynamics (CFD) Simulation of Test Chamber and Smoke-Generating Device

Michael J. Nusca

ARL-TR-663

January 1995

NOTICES

REPORT DOCUMENTATION PAGE	Form Approved OMB No. 0704-0188

1. AGENCY USE ONLY *(Leave blank)*	2. REPORT DATE	3. REPORT TYPE AND DATES COVERED
	January 1995	Final, December 1993–August 1994

4. TITLE AND SUBTITLE
Computational Fluid Dynamics (CFD) Simulation of Test Chamber and Smoke-Generating Device

5. FUNDING NUMBERS
PR: 1L162618A1FL

6. AUTHOR(S)
Michael J. Nusca

7. PERFORMING ORGANIZATION NAME(S) AND ADDRESS(ES)
U.S. Army Research Laboratory
ATTN: AMSRL-WT-PA
Aberdeen Proving Ground, MD 21005-5066

8. PERFORMING ORGANIZATION REPORT NUMBER

9. SPONSORING/MONITORING AGENCY NAME(S) AND ADDRESS(ES)
U.S. Army Research Laboratory
ATTN: AMSRL-OP-AP-L
Aberdeen Proving Ground, MD 21005-5066

10. SPONSORING/MONITORING AGENCY REPORT NUMBER
ARL-TR-663

11. SUPPLEMENTARY NOTES

12a. DISTRIBUTION/AVAILABILITY STATEMENT
Approved for public release; distribution is unlimited.

12b. DISTRIBUTION CODE

13. ABSTRACT *(Maximum 200 words)*

The U.S. Army Research Laboratory (ARL) has completed an initial investigation of the flow field within a typical U.S. Army Edgewood Research, Development, and Engineering Center (ERDEC) test chamber via numerical simulation. The ERDEC test chamber is designed to mix compressor-driven airflow with gas/solid effluent from a test article placed inside the chamber. An example of such a test article is a smoke generator, or smoke pot. Simulation of this flow utilized ARL computational fluid dynamics (CFD) codes that include multispecies chemical kinetics. Numerical solutions of the gas flow and effluent concentration distributions in the test chamber were generated for operating times up to 4.5 min. Numerical simulations reveal that certain values of chamber through-flow induce flow patterns within the chamber that are dominated by rotating vortices. This flow pattern increases the effluent residence time in the chamber as well as the mixing of gas/particulate from the test article with air. As a result, pockets of high effluent concentration can form in the chamber. Graphical results with discussion are presented.

14. SUBJECT TERMS
Navier-Stokes, computational fluid dynamics, turbulence, smoke, obscurants

15. NUMBER OF PAGES
35

16. PRICE CODE

17. SECURITY CLASSIFICATION OF REPORT	18. SECURITY CLASSIFICATION OF THIS PAGE	19. SECURITY CLASSIFICATION OF ABSTRACT	20. LIMITATION OF ABSTRACT
UNCLASSIFIED	UNCLASSIFIED	UNCLASSIFIED	SAR

INTENTIONALLY LEFT BLANK.

ACKNOWLEDGMENTS

Mr. Don Palughi and Mr. Larry Bickford of the Research and Technology Directorate of the U.S. Army Edgewood Research, Development, and Engineering Center (ERDEC) are acknowledged for supporting this effort and for providing technical assistance.

INTENTIONALLY LEFT BLANK.

TABLE OF CONTENTS

INTENTIONALLY LEFT BLANK.

LIST OF FIGURES

INTENTIONALLY LEFT BLANK.

1. INTRODUCTION

The U.S. Army Research Laboratory (ARL) completed an initial investigation of the flow field within a typical test chamber operated by the Army Edgewood Research, Development and Engineering Center (ERDEC). The ERDEC test chamber is designed to mix compressor-driven airflow with gas/solid effluent from a test article placed inside the chamber. An example of such a test article is a smoke generator, or smoke pot, commonly used on the battlefield to provide a means of obscurant. During the test, the air/effluent flow field is exhausted from the test chamber for analysis. In order to simulate this flow, the ARL applied computational fluid dynamics (CFD) codes that include multispecies chemical kinetics as well as multiphase (particulate) submodels. These codes were developed at ARL to numerically solve the Navier-Stokes equations and simulate the chemically reacting, multiphase flow field in gun propulsion systems. This code has been used successfully for other applications at ARL (Nusca 1989, 1991, 1993).

Application of the code to the present study involved generating a computational mesh that covered the chamber interior as well as specifying proper boundary conditions on the chamber walls, chamber top (air inflow), chamber exit (outflow), and test article (effluent outflow), as depicted in Figure 1. The governing equations, boundary conditions, and solution method are outlined in this report. Numerical solutions of the gas flow and effluent concentration distributions in the test chamber were generated for operating times up to 4.5 min. Graphical results with discussion are presented in this report. Numerical simulations reveal that certain values of chamber through-flow induce flow patterns within the chamber that are dominated by vortices. This flow pattern increases the effluent residence time in the chamber as well as the mixing of gas/particulate from the test article with air. The test article effluent jet feeds effluent into this vortical motion, and only that flow that is trapped near the chamber floor is drawn out of the chamber. Pockets of high effluent concentration can form in the chamber.

2. GOVERNING EQUATIONS

For purposes of producing a timely initial investigation, the cylindrical test chamber was modeled as two-dimensional (2D). The governing equations are written in Cartesian coordinates with velocity components u and v for the x (along chamber floor) and y (along chamber height) directions, respectively (see Figure 1). The Reynolds-Averaged Navier-Stokes (RANS) equations describe the 2D reacting gas flow (N species mixture) in the chamber given conditions at the boundaries of the geometry. These partial differential equations describe the time (t) evolution of the dependent variables of velocity (u, v), pressure

(p), mixture density (ρ), species mass fraction (σ_i, for i = 1 to N species), internal energy (e), temperature (T, derived from energy), and viscous shear stresses (τ).

$$\frac{\partial W}{\partial t} + \frac{\partial (F_1 - G_1)}{\partial x} + \frac{\partial (F_2 - G_2)}{\partial y} = \Omega. \tag{1}$$

$$W = \left[e, \rho, \rho u, \rho v, \rho\sigma_1, \ldots, \rho\sigma_{N-1}\right].$$

$$F_1 = \left[(e+p)\, u, \rho u, \rho u^2 + p, \rho u v, \rho u \sigma_1, \ldots, \rho u \sigma_{N-1}\right].$$

$$F_2 = \left[(e+p)\, v, \rho v, \rho v u, \rho v^2 + p, \rho v \sigma_1, \ldots, \rho v \sigma_{N-1}\right].$$

$$\Omega = \left[0, 0, 0, 0, \textstyle\sum_k \omega_{1k}, \ldots, \sum_k \omega_{(N-1)k}\right].$$

$$G_1 = \left[\kappa_m \frac{\partial T}{\partial x} + \sum_i \rho D (h_i - h_N) \frac{\partial \sigma_i}{\partial x} + u\,\tau_{xx} + v\,\tau_{xy}, 0, \tau_{xx}, \tau_{xy}, \rho D \frac{\partial \sigma_1}{\partial x}, \ldots, \rho D \frac{\partial \sigma_{N-1}}{\partial x}\right].$$

$$G_2 = \left[\kappa_m \frac{\partial T}{\partial y} + \sum_i \rho D (h_i - h_N) \frac{\partial \sigma_i}{\partial y} + u\tau_{yx} + v\tau_{yy}, 0, \tau_{yx}, \tau_{yy}, \rho D \frac{\partial \sigma_1}{\partial y}, \ldots, \rho D \frac{\partial \sigma_{N-1}}{\partial y}\right].$$

The shear stress terms are given by

$$\tau_{xx} = 2\mu_m \frac{\partial u}{\partial x} - \frac{2\mu_m}{3}\left(\frac{\partial u}{\partial x} + \frac{\partial v}{\partial y}\right),\ \tau_{yy} = 2\mu_m \frac{\partial v}{\partial y} - \frac{2\mu_m}{3}\left(\frac{\partial u}{\partial x} + \frac{\partial v}{\partial y}\right),\ \tau_{yx} = \mu_m\left(\frac{\partial u}{\partial y} + \frac{\partial v}{\partial x}\right).$$

In these equations, σ_i and ω_i are the mass fraction and chemical production terms for the i^{th} species. For the present application, finite-rate chemical production terms were not used. Chemical reaction was modeled as an infinitely fast, one-step, unidirectional (i.e., forward) reaction of smoke pot effluent (i = 1) and air (i = 2) to form product (i = 3) for stoichiometric air/effluent ratio of 0.17 and effluent density above 50 g/m^3. The reaction temperature was taken as 680° C.

$$\text{Effluent} + \text{Air} \rightarrow \text{Product}$$

$$\frac{\omega_1}{M_1} = -k_f \frac{\rho\sigma_1}{M_1}\frac{\rho\sigma_2}{M_2}, \quad \frac{\omega_2}{M_2} = -k_f \frac{\rho\sigma_1}{M_1}\frac{\rho\sigma_2}{M_2}, \quad \frac{\omega_3}{M_3} = +k_f \frac{\rho\sigma_1}{M_1}\frac{\rho\sigma_2}{M_2} .$$

$$k_f = 1 \times 10^{20} .$$

The temperature dependence of the species viscosity, μ_i, and thermal conductivity, κ_i, can be modeled using Sutherland's law (White 1974),

$$\frac{\mu_i}{\mu_{oi}} = \left(\frac{T}{T_{o\mu}}\right)^{3/2} \frac{T_{o\mu} + S_\mu}{T + S_\mu}, \quad \frac{\kappa_i}{\kappa_{oi}}\left(\frac{T}{T_{o\kappa}}\right)^{3/2} \frac{T_{o\kappa} + S_\kappa}{T + S_\kappa} .$$

The terms μ_o, T_o, and S can vary with species but were assumed to be constant with values of S_μ = 199 R, $T_{o\mu}$ = 491.6 R, μ_o = 0.1716 mP, S_κ = 350 R, $T_{o\kappa}$ = 491.6 R, κ_o = 0.0139 BTU/h-ft-R. The mixture viscosity and thermal conductivity (mixture quantities are denoted by subscript m) are determined using Wilke's law (Wilke 1950), denoting f as μ or κ,

$$f_m = \sum_i \left[X_i f_i \left(\sum_j X_j \phi_{ij}\right)^{-1}\right], \quad \phi_{ij} = \frac{1}{\sqrt{8}}\left(1 + \frac{M_i}{M_j}\right)^{-1/2}\left[1 + \left(\frac{f_i}{f_j}\right)^{1/2}\left(\frac{M_j}{M_i}\right)^{1/4}\right]^2 ,$$

where X_i and M_i are the mole fraction ($X_i = \rho\sigma_i/M_i$) and molecular weight of the i^{th} species, respectively (M_1 = 97.94, M_2 = 28.8, and M_3 = 63.37 g/mole). Fick's law (White 1974) is used to relate the mixture diffusivity to the mixture viscosity through the Schmidt number, Sc = $\mu_m/(\rho\ D)$, assumed unity. The specific heat at constant pressure of each species (per mass) is generally given by the following fourth-order polynomial curve fit (Drummond, Rogers, and Hussaini 1987):

$$\frac{c_{p_i}}{R_i} = A_i + B_i T + C_i T^2 + D_i T^3 + E_i T^4 .$$

For the present study, c_p was assumed constant with values c_{p1} = 0.2878, c_{p2} = 0.238, and c_{p3} = 0.1277 cal/g°C. The mixture pressure (equation of state), enthalpy, total energy per unit volume,

and ratio of specific heats are given by (R_u is the universal gas constant and ΔH_{fi} is the heat of formation for species i)

$$p = \sum_i p_i = \rho T R_u \sum_i \frac{\sigma_i}{M_i} ,$$

$$h = \sum_i \sigma_i \int^T c_{p_i} dT + \sum_i \sigma_i \Delta H_{f_i} ,$$

$$e = \frac{p}{\gamma - 1} + \rho \frac{\left(u^2 + v^2\right)}{2} + \sum_i \rho \sigma_i \Delta H_{f_i} ,$$

$$\gamma = 1 + \left[\frac{c_{p_m}}{R_u \sum_i \left(\sigma_i / M_i\right)} - 1 \right]^{-1} ,$$

and

$$c_{p_m} = \frac{1}{T} \sum_i \sigma_i \int^T c_{p_i} dT .$$

An algebraic turbulence model (Bradshaw, Cebeci, and Whitelaw 1981) was used. In this model, the eddy viscosity, μ_t, is computed assuming that the viscous layer consists of an inner and an outer component. The inner region follows the Prandtl mixing length formulation based on a prescribed characteristic length scale, L, a boundary layer intermittency factor, ε (having a value of 0 for laminar, 1 for turbulent flows, and a function of x for transitional flows), the displacement thickness of the layer, δ, and a constant, a.

$$\left(\mu_t\right)_{\text{inner}} = L^2 y \, \| \frac{\partial u}{\partial y} \| , \; 0 \le y \le y_c .$$

$$\left(\mu_t\right)_{\text{outer}} = a u_e \, \| \delta \| \, \varepsilon , \; y_c \le y \le y_e .$$

Here, y_c, is a prescribed, small distance from the solid boundary, and y_e is the edge of the viscous layer. Further details can be obtained from Bradshaw, Cebeci, and Whitelaw (1981). The fluid viscosity is then $\mu = \mu_m(T) + \mu_t$, where $\mu_m(T)$ is obtained using Sutherland's law and Wilke's law.

3. BOUNDARY CONDITIONS AND INITIAL CONDITIONS

The boundaries of the test chamber (see Figure 1) are the air inlet at the top (roof), the exit port on the chamber floor (connected by ducts to the wind tunnel fan), and the vertical walls. The smoke pot is placed on the chamber floor, near the chamber exit port. Since the governing equations are elliptic (low-speed flow), conditions along these boundaries must prescribe values of the dependent variables, the gradient of the dependent variables in the boundary-normal direction, or an algebraic relation which connects the values of the dependent variables to the normal component of velocity.

At the air inlet, x-direction profiles of all dependent variables, p, u, v, σ, T, and ρ, are specified. It is assumed that the flow at the inlet consists of air and that convection/diffusion of effluent to the chamber top is not permitted to exit the chamber. By mass conservation, the inlet flow velocity was specified as $u = .062$ ft/s, and a parabolic-shaped profile was assumed.

The exit port velocity was specified as $u = 2.96$ ft/s (5,380 l/min) with a parabolic-shaped profile. Boundary-normal gradients of all dependent variables at the exit plane are zero. Mass that exits the port is not assumed to reenter.

The no-slip/no-penetration condition ($u = v = 0$) is applied to the solid chamber and smoke pot walls. The walls are assumed to be adiabatic (i.e, normal derivative of T set to zero). The normal gradient of all mass fractions, $\partial\sigma_i/\partial n$, are also set to zero.

The top of the smoke pot was assumed to be a constant mass flux source of effluent with $u = 12.7$ ft/s, $T = 320^\circ$ C, $M_1 = 97.94$ g/mole, and $c_p = 0.2878$ cal/g$^\circ$ C.

4. COMPUTATIONAL ALGORITHM

Equation (1) can be reduced to a successive-substitution formula for a general dependent variable, W, at each node on the computational grid. Central finite-differences are used for the diffusive (arrays G_1

and G_2) and source terms (array Ω) and upwind differences for the convective terms (arrays F_1 and F_2). Using upwind differencing in the species conservation equations (i.e., $W = \rho\sigma_i$) reduces the occurrence of negative species mass fractions in mixing layers. The resulting system of equations for the entire grid is solved using a Gauss-Seidel relaxation scheme. Each iteration cycle is made up of J subcycles, where J is the number of equations being considered. In each subcycle, grid points are scanned row by row, and a single variable is updated. When all subcycles are completed, a new iteration cycle in which the values of the variables from the latest iteration are immediately used is started. This is consistent with the Gauss-Seidel methodology. Convergence is satisfied when the greatest relative change in any flow variable is smaller than a prescribed tolerance. See Nusca (1989, 1991) for further details.

5. RESULTS AND DISCUSSION

Figure 1 shows the computational grid used to discretize the chamber interior. The number of grid nodes in the x and y directions are 75 and 50, respectively (3,750 nodes total). Grid node clustering was used to resolve flow gradients near the smoke pot.

The simulation was run for approximately 1 min to establish steady flow in the chamber before the smoke pot was activated. Figure 2 shows the streamline (contour lines of constant stream function) patterns. Note that a large counterclockwise vortex resides to the upper left of the smoke pot (established by flow from the chamber inlet that must turn at the chamber floor) and that a smaller clockwise vortex resides over the smoke pot (established by flow rising in the vertical direction that is turned by the chamber inlet flow at the top).

Figures 3, 4, 5, and 6 show the flow streamline pattern after 1, 2, 3, and 4 min of smoke pot operation, respectively. Initially, flow from the smoke pot rises toward the chamber top, establishing two small vortices near the pot, rotating in opposite directions. At later times, the flow settles into a large counterclockwise vortex offset from the centerline of the chamber and fed by the smoke pot jet. Flow entrained in the chamber exit port is limited to that trapped near the chamber floor. Figure 7 shows the flow streamline pattern at 4.5 min, which is 0.5 min after the smoke pot has ceased operation. The vortex has reduced in size and is centered between the vertical chamber walls.

Figures 8–12 and Figures 13–17 show contours of smoke pot effluent mass fraction, σ_1, (mass of effluent/total mass) and effluent density (product of mass fraction and mixture density), respectively, at

times 1–4.5 min. At early times, effluent concentrations are high in the smoke pot jet. At later times, the effluent is entrained in the chamber vortex and diffused to smaller concentrations. Even at later times, pockets of high concentration (50 g/m^3 or greater) can be noted. The flow pattern is not greatly disturbed by the chamber exit port on the floor. Figures 12 and 17 show the effluent mass fraction and density at 4.5 min, 0.5 min after flow from the smoke pot has been stopped. The chamber vortex has swept effluent into the vicinity of the smoke pot where it becomes trapped at large concentration levels.

6. CONCLUSIONS

Due to the low-vertical flow velocity (0.06–2.7 ft/s) through the chamber induced by the small chamber exit port on the floor, the natural flow pattern in the chamber is one that is dominated by rotating vortices. This pattern increases the flow residence time in the chamber and mixes gases from the smoke pot with air (similar to a "well-stirred reactor"). The smoke pot jet feeds effluent into this vortical motion, with only that flow that is trapped near the chamber floor exiting the chamber. As a result, effluent is allowed to form pockets of high concentration that may chemically react with the fresh-air supply fed from the chamber inlet (i.e, top). After the smoke pot ceases operation, the chamber vortex concentrates effluent near the chamber wall. A larger chamber exit port and forced exit velocity (controlled by the wind tunnel fan) may assist in breaking these vortices and evacuating the chamber at the higher rate. The increased chamber through-flow should be sufficient to turn the smoke pot jet toward the exit. Numerical simulations aimed at predicting this effect have not been pursued.

The numerical simulations, results, discussions, and conclusions reached in this report are subject to the assumptions used in the model and the information supplied to the model in the form of boundary conditions. While the confidence level in the model is high (based on performance in simulating other problems), further studies that test model sensitivity to the supplied boundary conditions should be conducted. A full three-dimensional simulation should be conducted to model the perforated chamber top wall, in addition to three discrete smoke pot exit holes as well as flow obstructions (i.e., pipes) in the chamber. These are thought to represent secondary effects in the simulation of unknown final effect on the results.

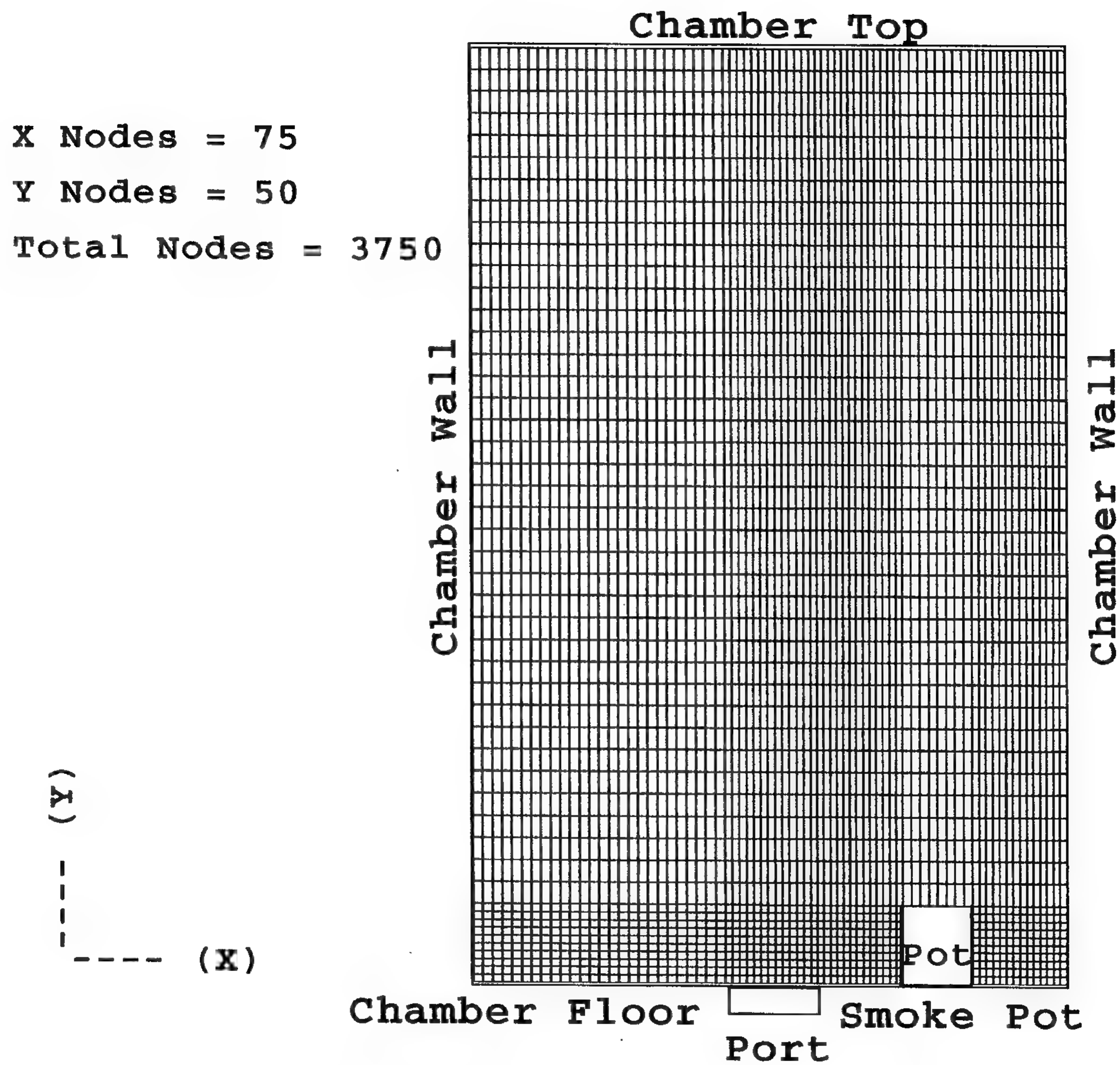

Figure 1. Schematic of test chamber and smoke pot showing computational grid.

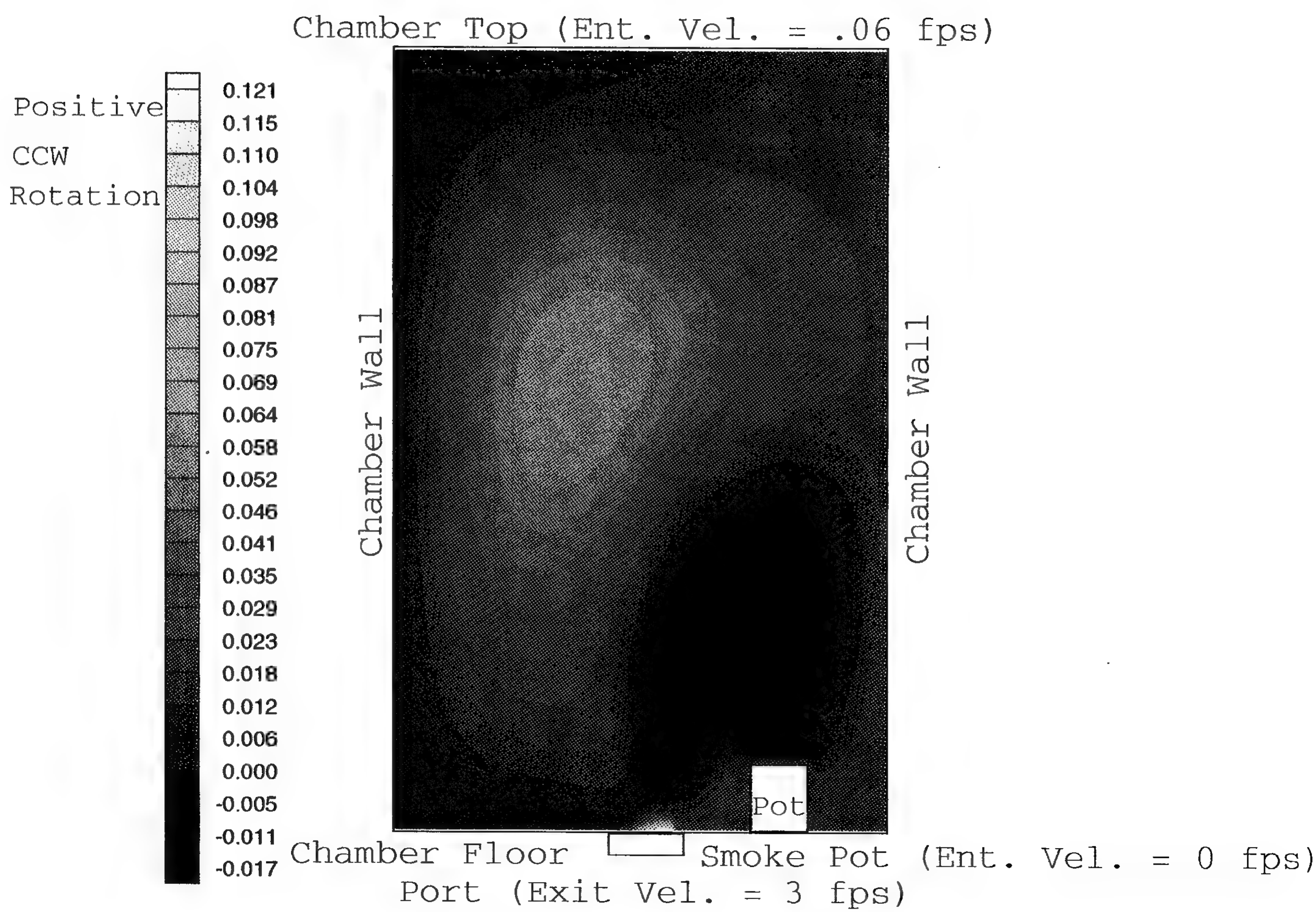

Figure 2. Stream function contours before smoke pot operation.

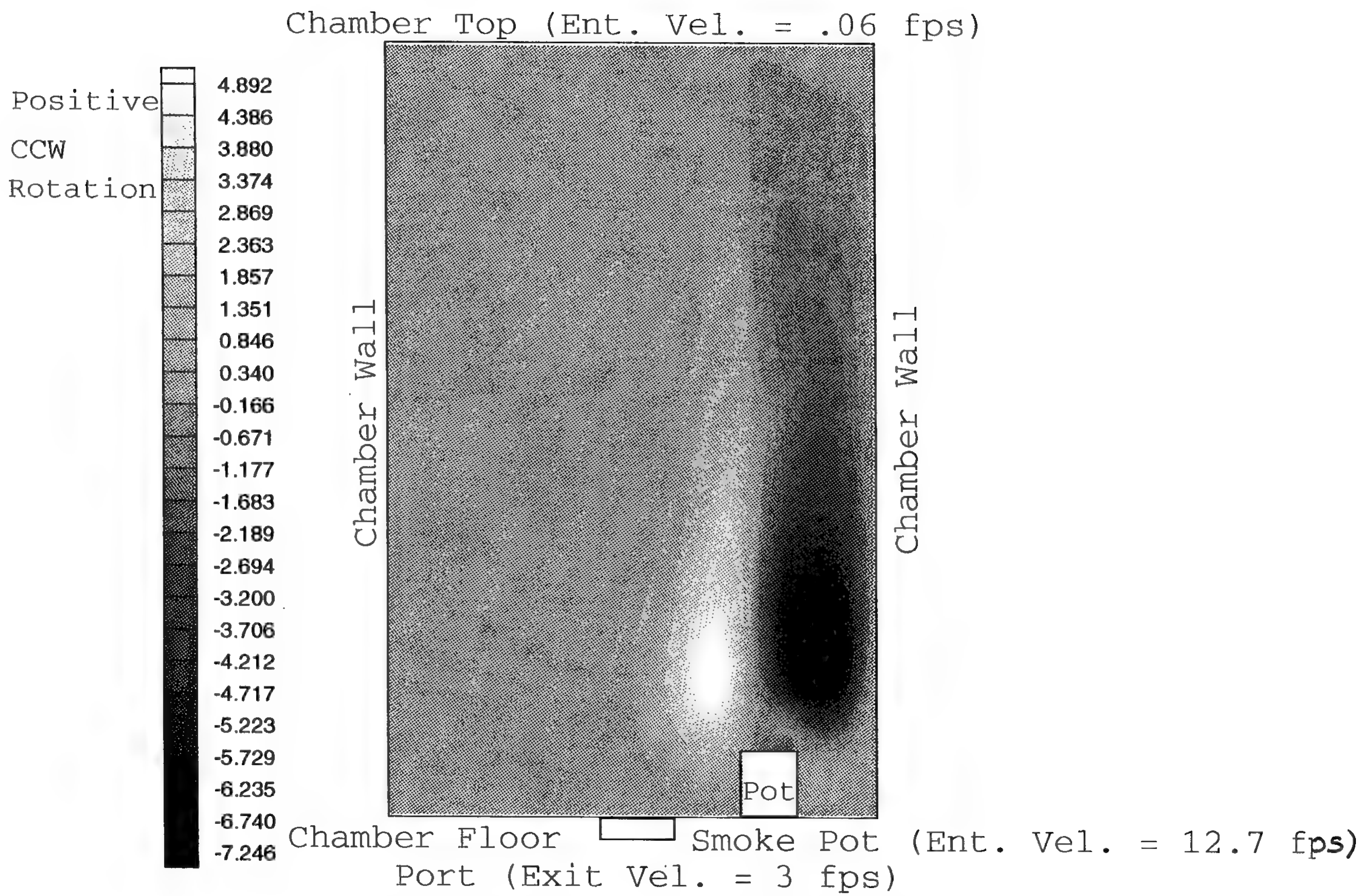

Figure 3. Stream function contours 1.0 min after smoke pot startup.

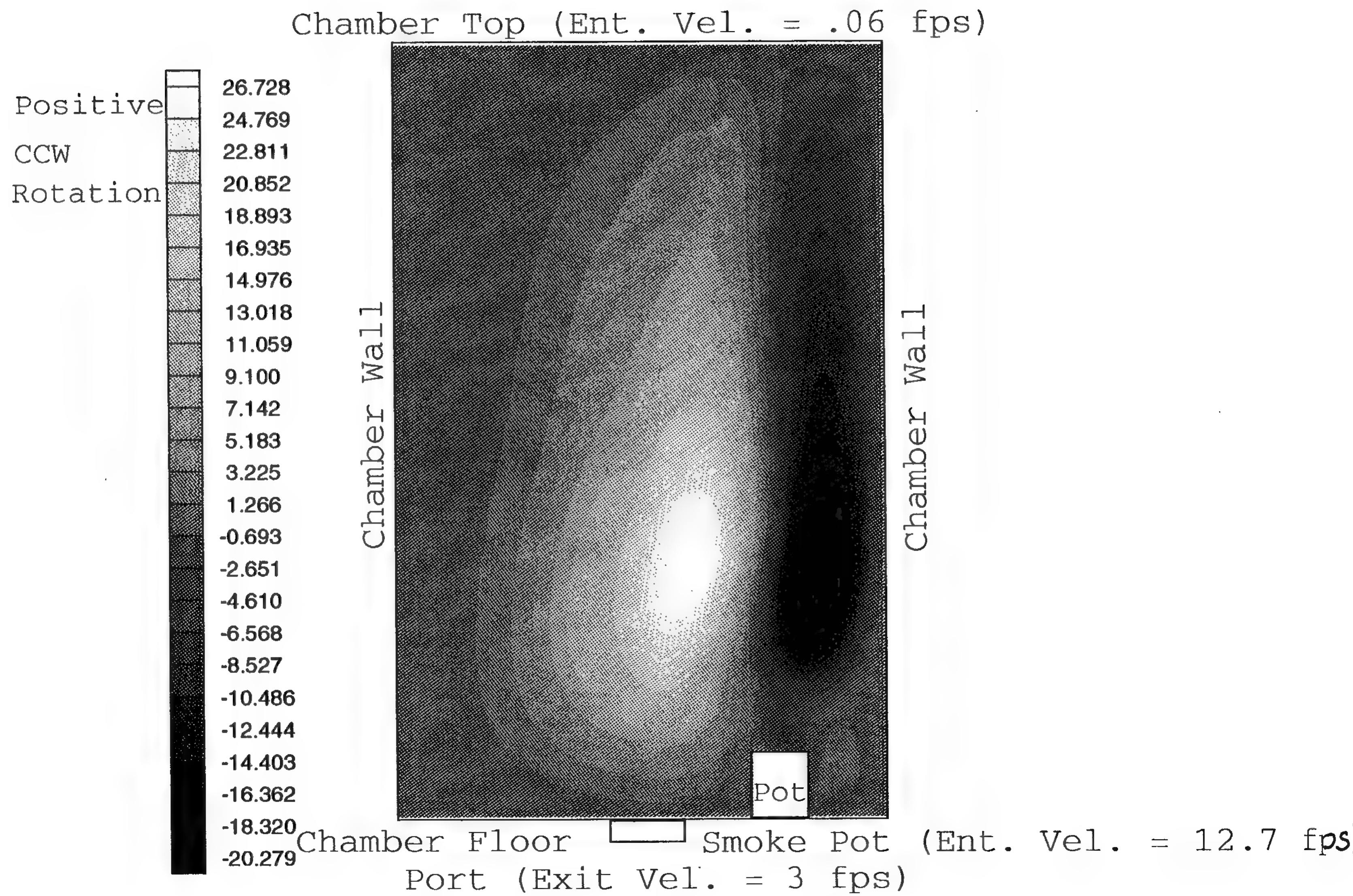

Figure 4. <u>Stream function contours 2.0 min after smoke pot startup.</u>

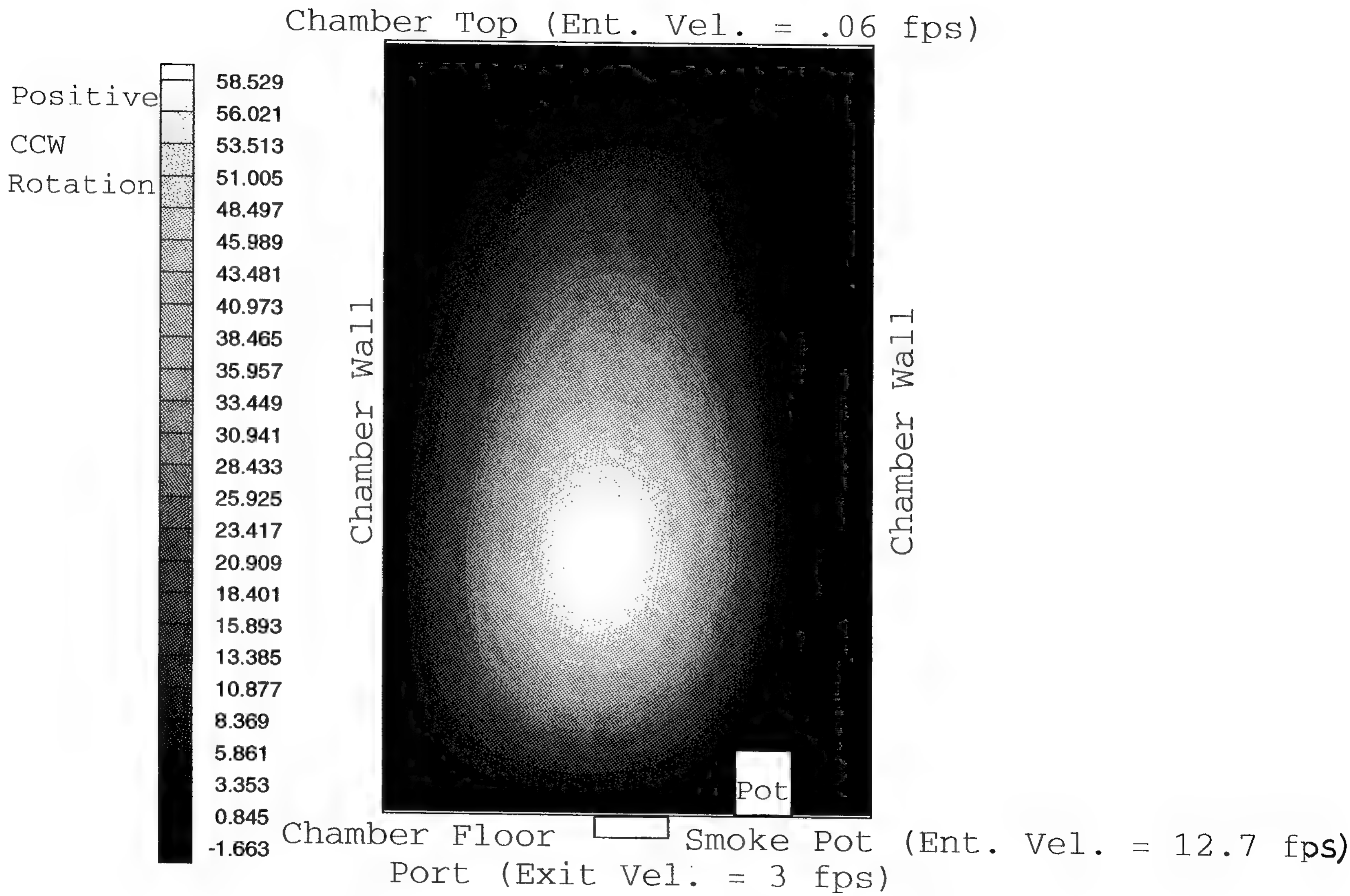

Figure 5. Stream function contours 3.0 min after smoke pot startup.

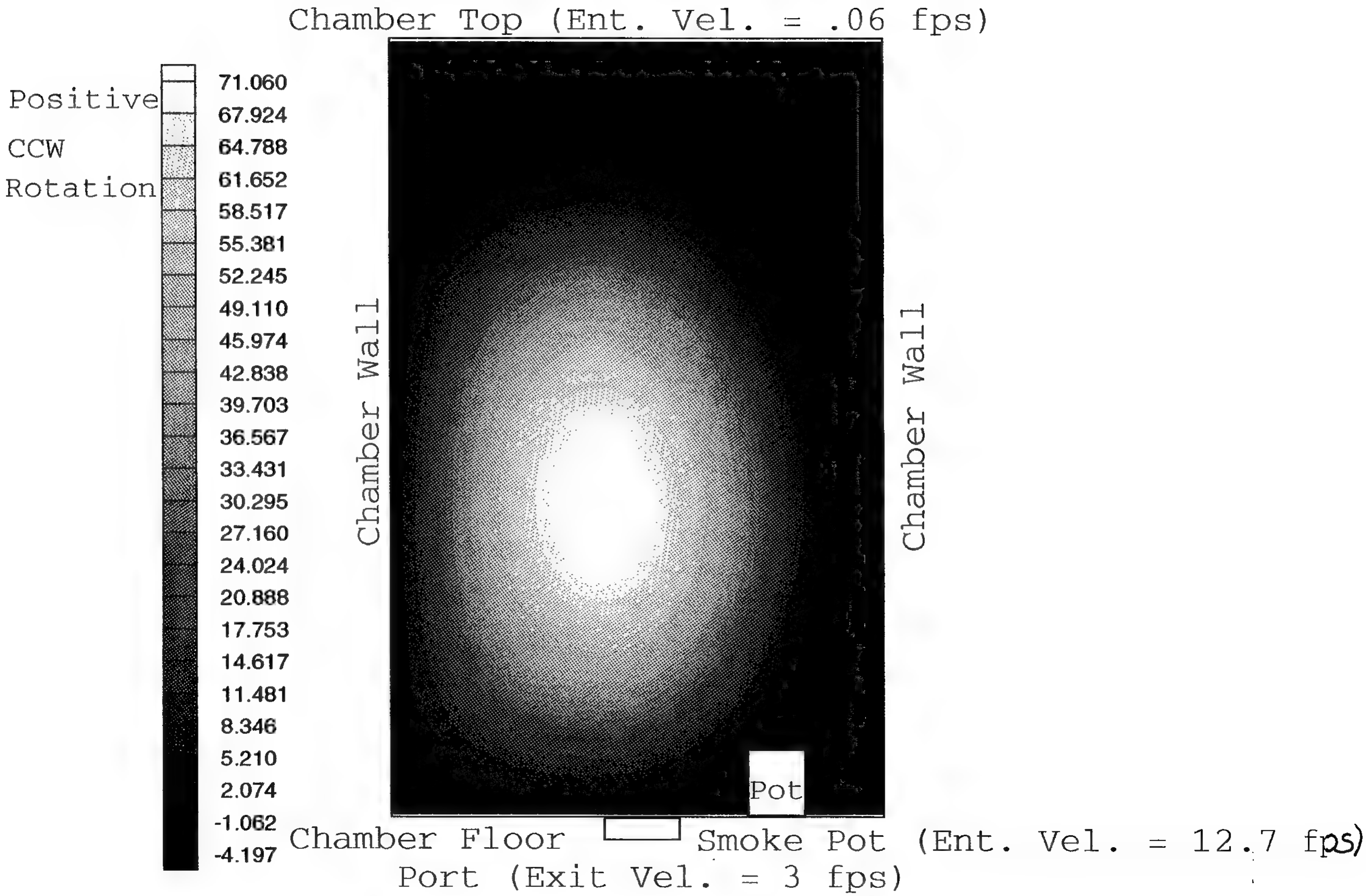

Figure 6. Stream function contours 4.0 min after smoke pot startup.

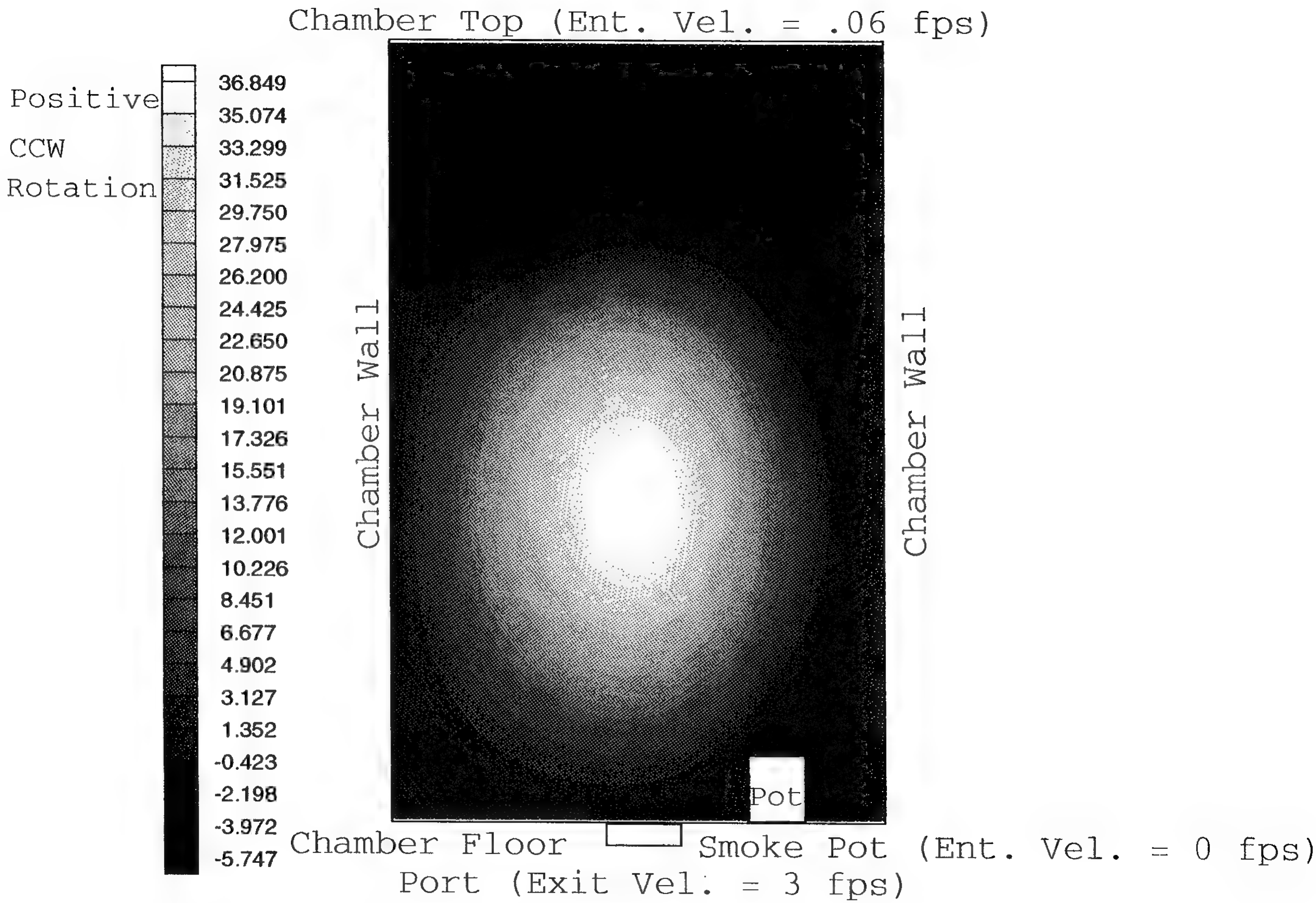

Figure 7. Stream function contours 4.5 min after smoke pot startup, 0.5 min after smoke pot termination.

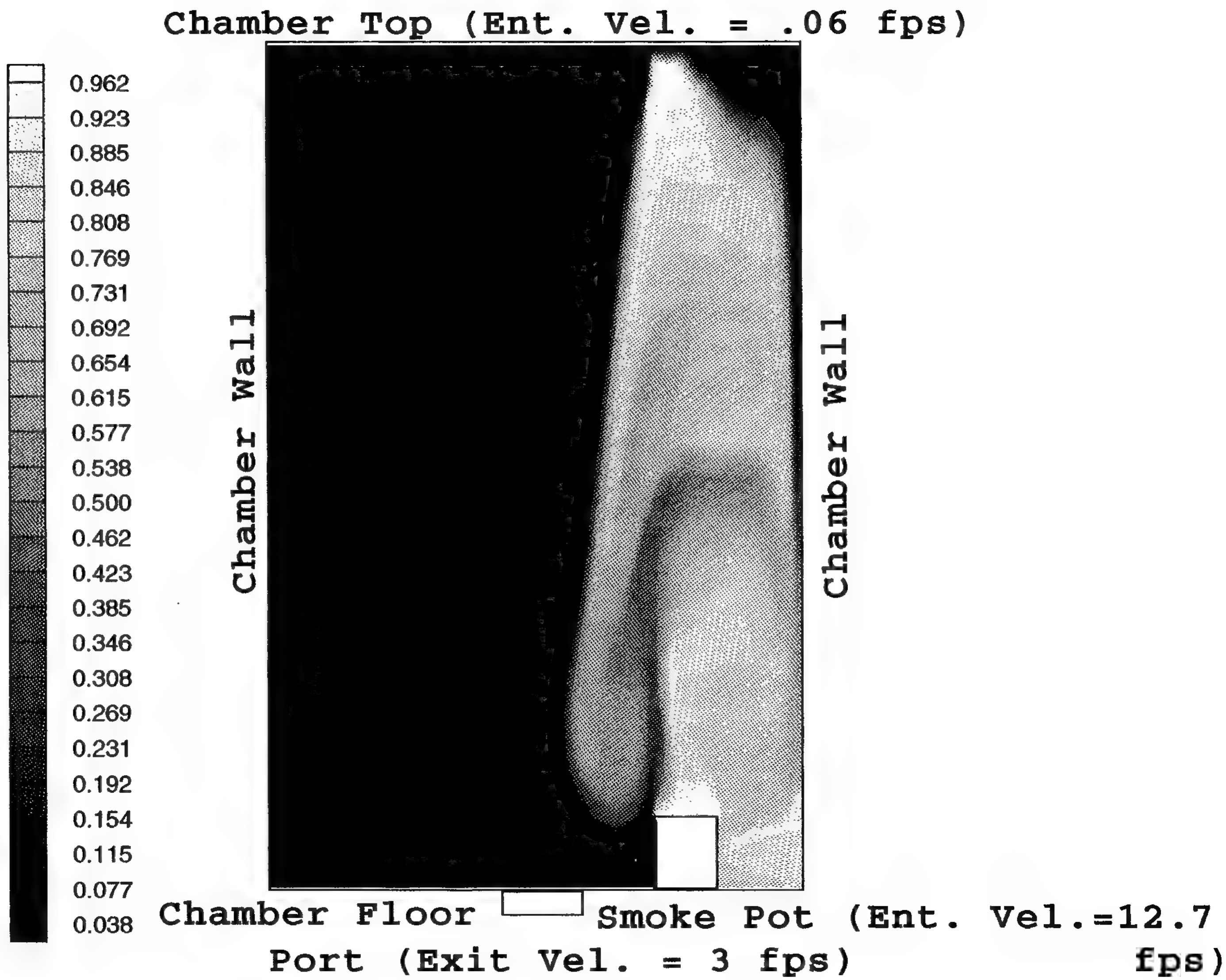

Figure 8. Effluent mass fraction contours 1.0 min after smoke pot startup.

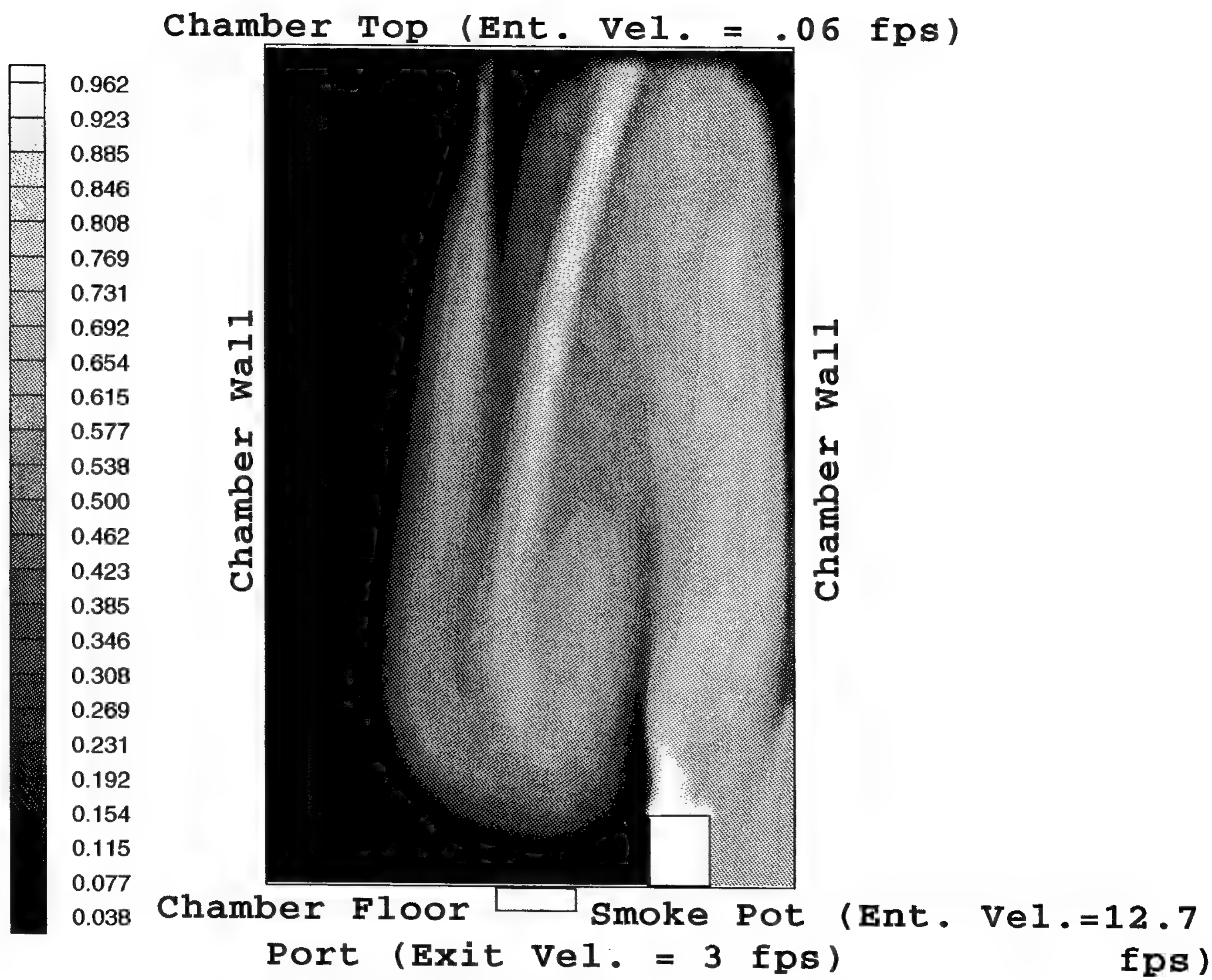

Figure 9. Effluent mass fraction contours 2.0 min after smoke pot startup.

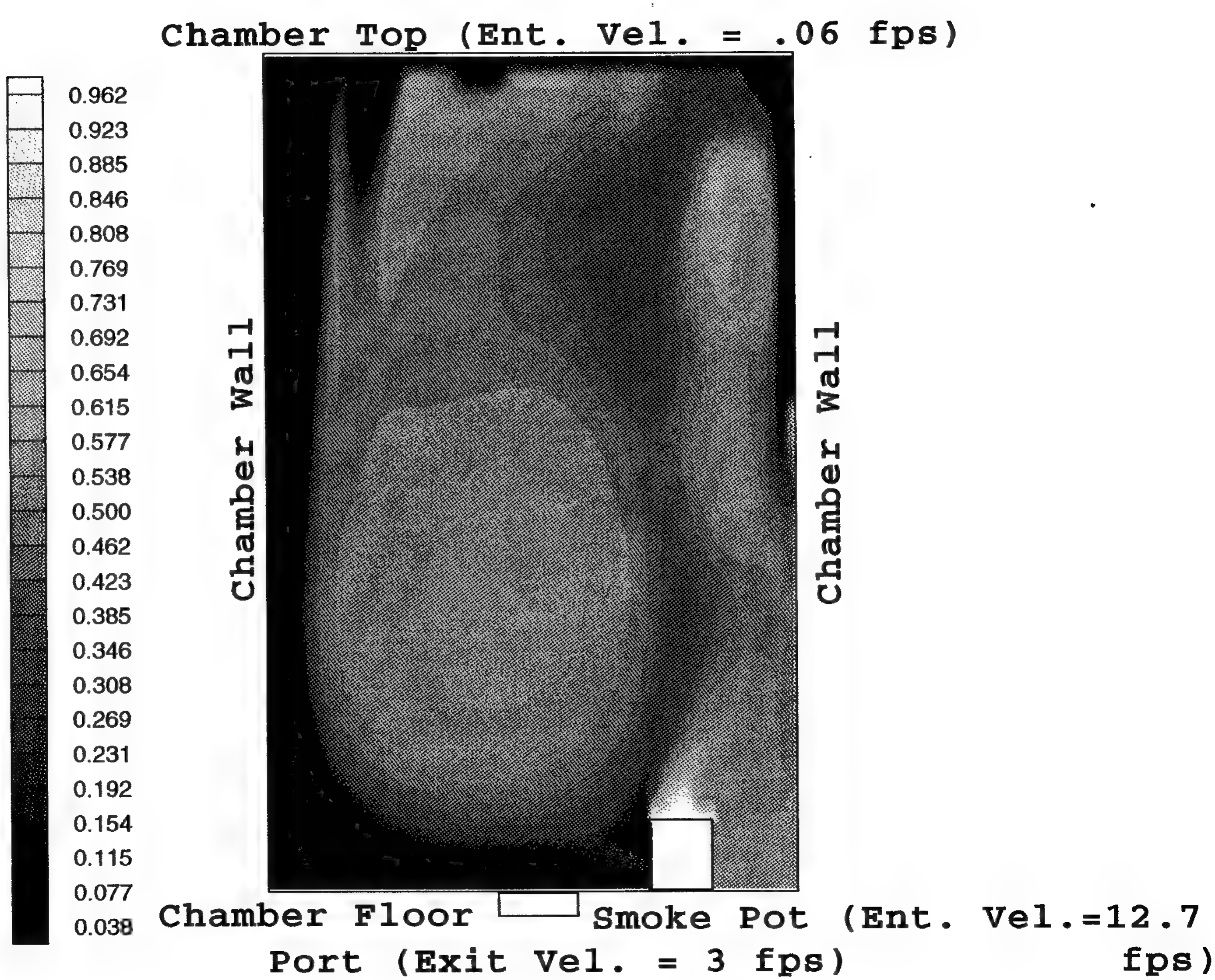

Figure 10. Effluent mass fraction contours 3.0 min after smoke pot startup.

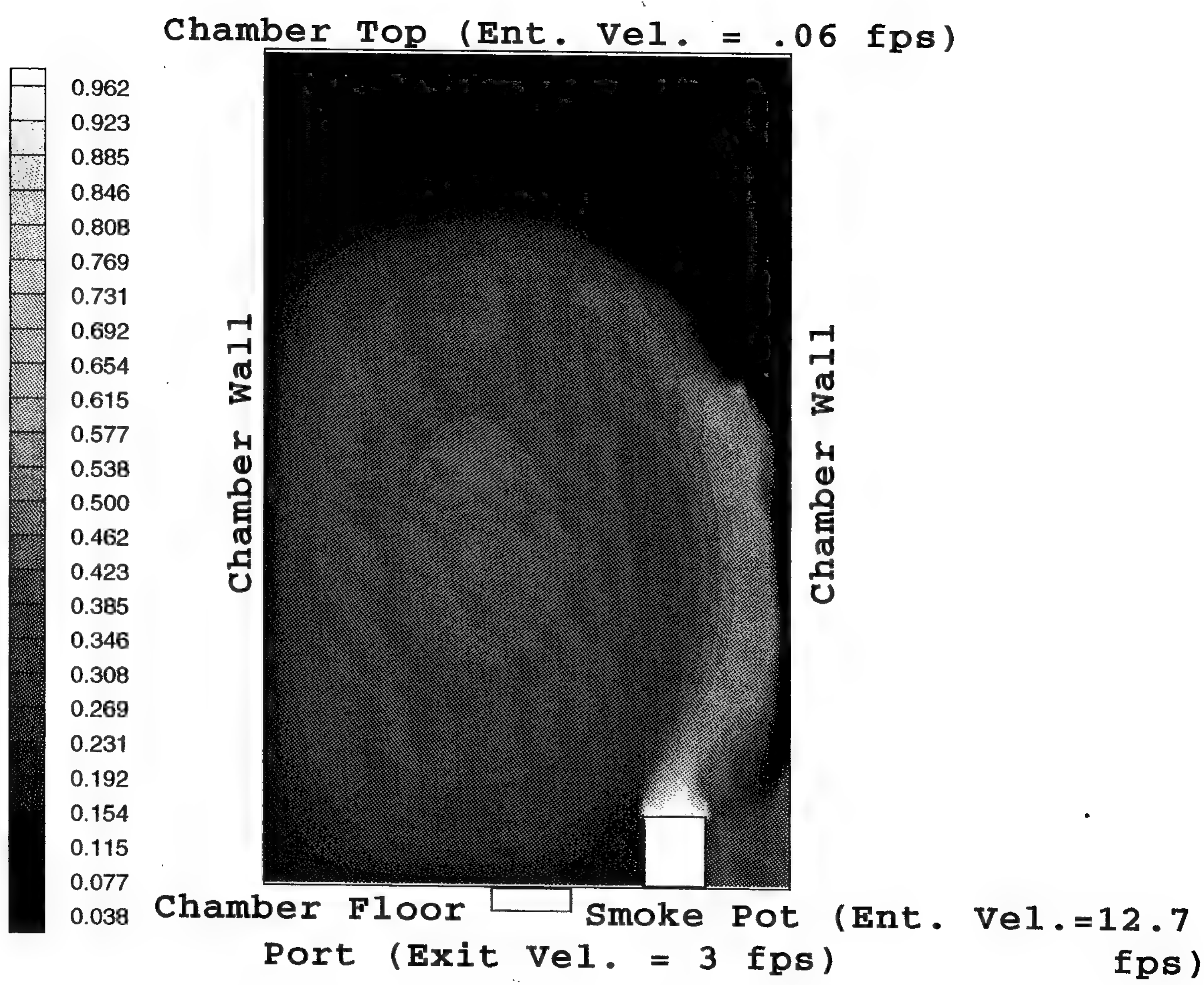

Figure 11. Effluent mass fraction contours 4.0 min after smoke pot startup.

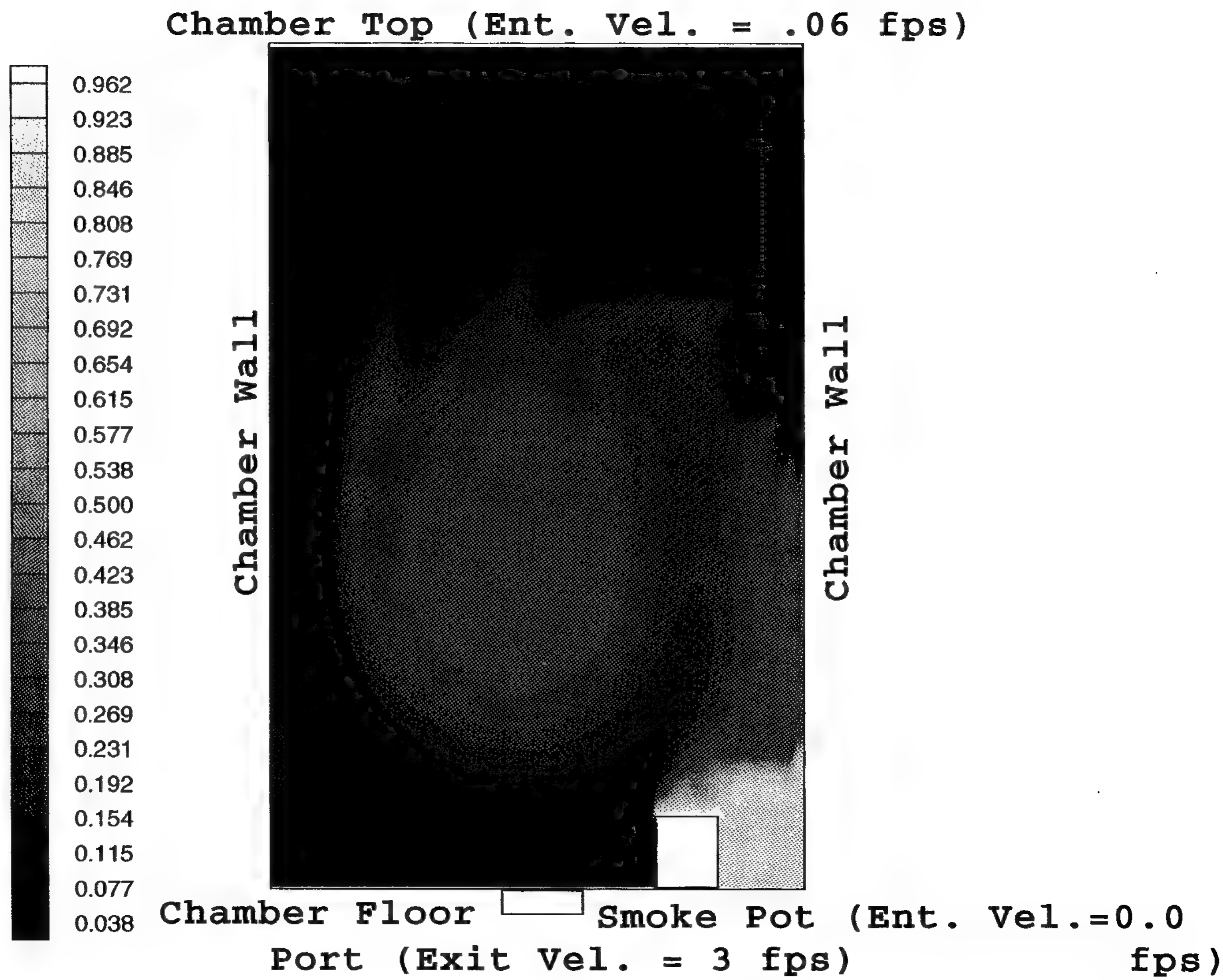

Figure 12. Effluent mass fraction contours 4.5 min after smoke pot startup, 0.5 min after smoke pot termination.

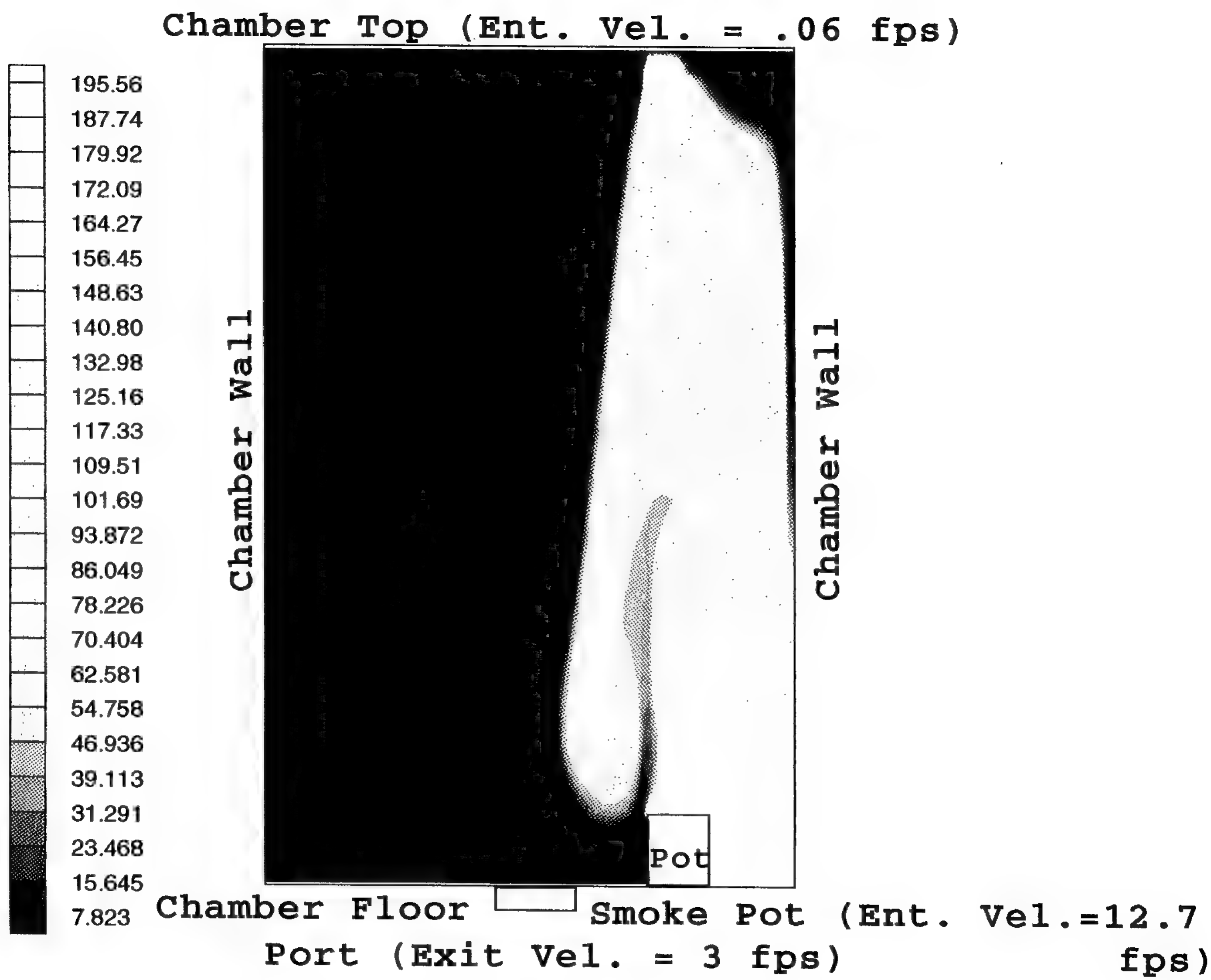

Figure 13. Effluent density (g/m^3) contours 1.0 min after smoke pot startup.

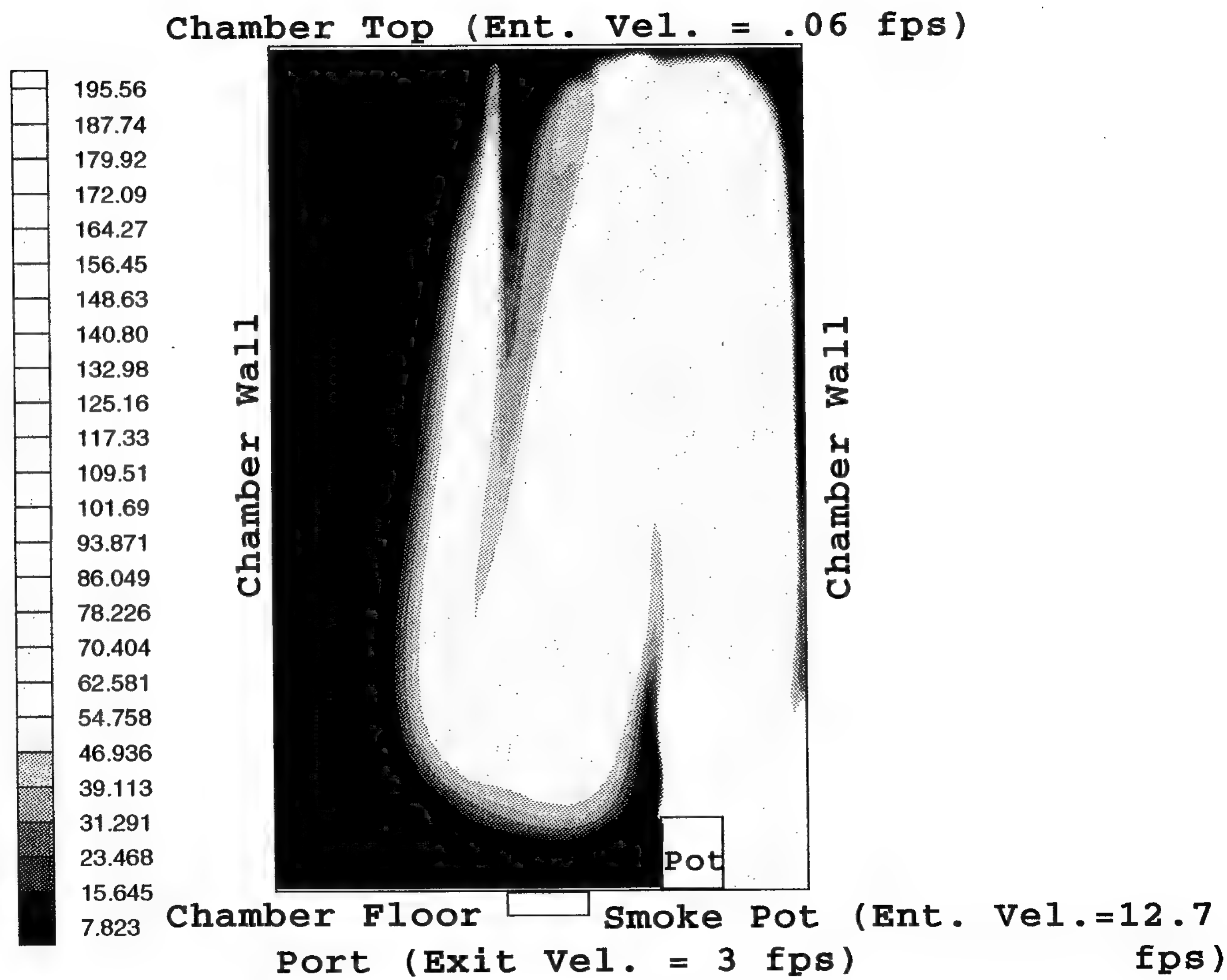

Figure 14. Effluent density (g/m^3) contours 2.0 min after smoke pot startup.

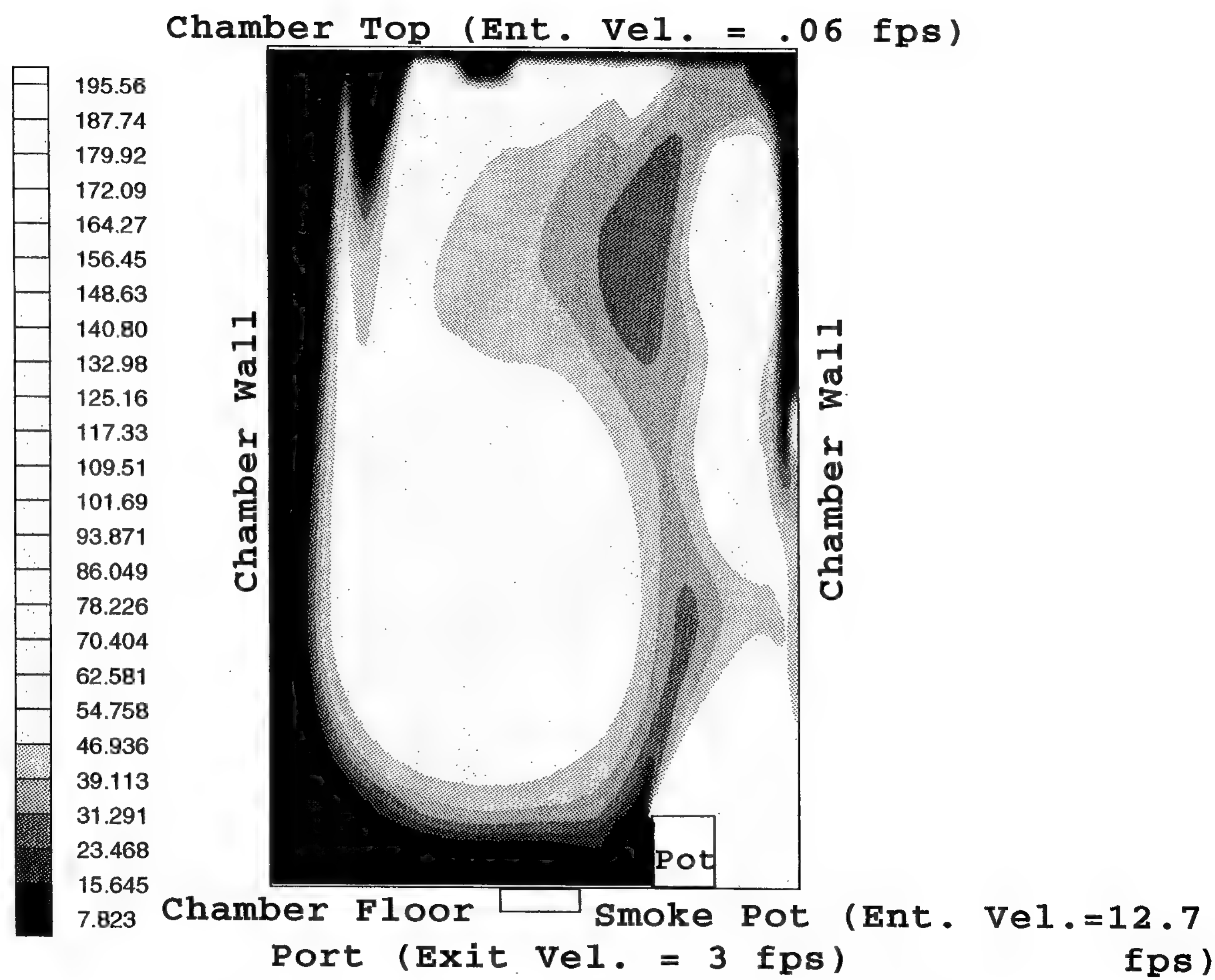

Figure 15. Effluent density (g/m^3) contours 3.0 min after smoke pot startup.

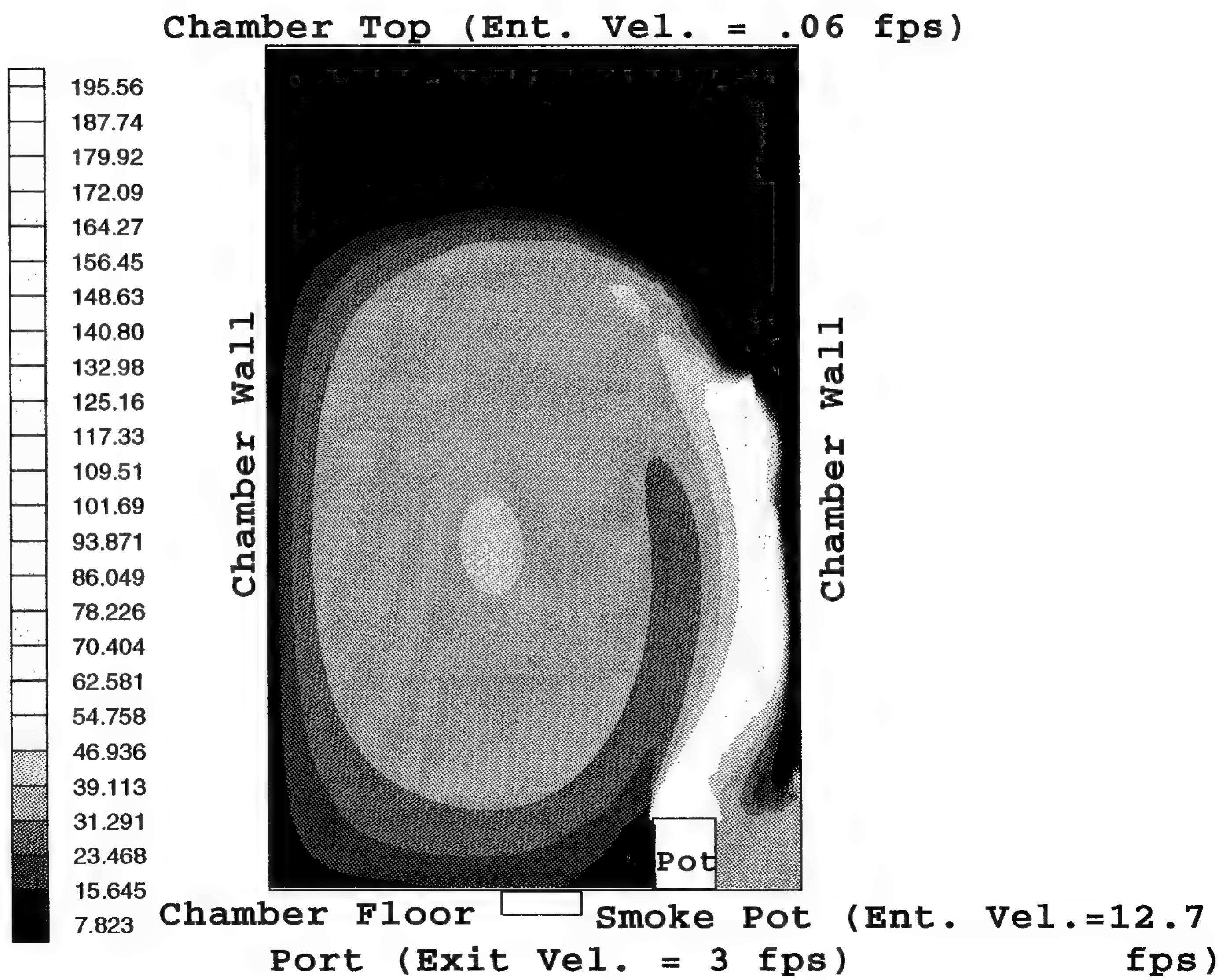

Figure 16. Effluent density (g/m^3) contours 4.0 min after smoke pot startup.

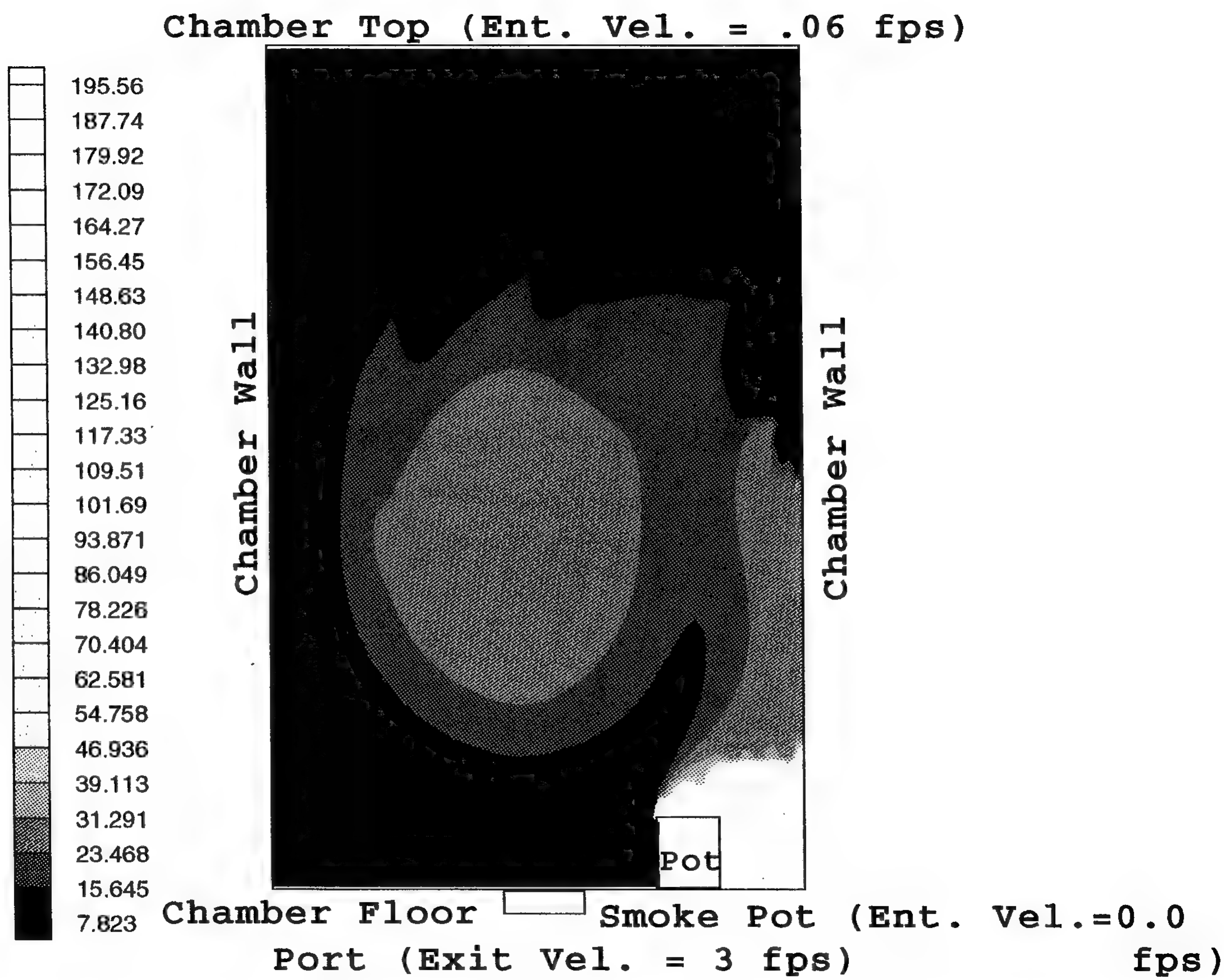

Figure 17. Effluent density (g/m^3) contours 4.5 min after smoke pot startup, 0.5 min after smoke pot termination.

7. REFERENCES

Baldwin, B. S., and H. Lomax. "Thin-Layer Approximation and Algebraic Model for Separated Turbulent Flows." AIAA Paper No. 78-257, January 1978.

Bradshaw, P., T. Cebeci, and J. H. Whitelaw. Engineering Calculation Methods for Turbulent Flow. New York: Academic Press, 1981.

Drummond, J. P, C. Rogers, and M. Y. Hussaini. "A Numerical Model for Supersonic-Reacting Mixing Layers." Computer Methods in Applied Mechanics and Engineering, vol. 64, 1987.

Nusca, M. J. "Steady Flow Combustion Model for Solid-Fuel Ramjet Projectiles." BRL-TR-2987, U.S. Army Ballistic Research Laboratory, Aberdeen Proving Ground, MD, April 1989.

Nusca, M. J. "Numerical Simulation of Reacting Flow in a Thermally Choked Ram Accelerator -- Model Development and Validation." BRL-TR-3222, U.S. Army Ballistic Research Laboratory, Aberdeen Proving Ground, MD, April 1991.

Nusca, M. J. "Numerical Simulation of Fluid Dynamics and Payload Dissemination in a Dual-Chamber Grenade." ARL-TR-77, U.S. Army Research Laboratory, Aberdeen Proving Ground, MD, February 1993.

White, F. M. Viscous Fluid Flow. New York: McGraw-Hill Book Co., 1974.

Wilke, C. R. "A Viscosity Equation for Gas Mixtures." Journal of Chemistry and Physics, vol. 18, no. 4, pp. 517–519, 1950.

INTENTIONALLY LEFT BLANK.

LIST OF SYMBOLS

c_p	=	specific heat capacity, constant p
c_v	=	specific heat capacity, constant volume
D	=	mass diffusion coefficient
e	=	specific total internal energy
F, G	=	flux vectors
h	=	molar specific enthalpy
L	=	Prandtl mixing length
M	=	molecular weight
N	=	total number of species
p	=	static pressure
R	=	specific gas constant, $(\gamma-1)c_p/\gamma$
R_u	=	universal gas constant, $R\ M_m$
Sc	=	Schmidt Number, $\mu_m/\rho\ D$
t	=	time
T	=	static temperature
u	=	axial velocity
v	=	radial velocity
W	=	dependent variable vector
x, y	=	Cartesian coordinates
X	=	species mole fraction

Greek Symbols

γ	=	ratio of specific heats, c_p/c_v
ΔH_f	=	enthalpy of formation
δ	=	boundary layer displacement thickness
ε	=	boundary layer intermittency factor
κ	=	heat transfer coefficient
μ	=	molecular viscosity

ρ = density

σ = species mass fraction

τ = shear stress tensor

ω = chemical production term

Ω = source term vector

<u>Subscripts</u>

e = edge of the viscous layer

i = i^{th} species

m = mixture quantity

p = constant pressure

t = turbulence quantity

v = constant volume

x = x-direction

y = y-direction

NO. OF COPIES	ORGANIZATION
2	ADMINISTRATOR ATTN DTIC DDA DEFENSE TECHNICAL INFO CTR CAMERON STATION ALEXANDRIA VA 22304-6145
1	COMMANDER ATTN AMCAM US ARMY MATERIEL COMMAND 5001 EISENHOWER AVE ALEXANDRIA VA 22333-0001
1	DIRECTOR ATTN AMSRL OP SD TA US ARMY RESEARCH LAB 2800 POWDER MILL RD ADELPHI MD 20783-1145
3	DIRECTOR ATTN AMSRL OP SD TL US ARMY RESEARCH LAB 2800 POWDER MILL RD ADELPHI MD 20783-1145
1	DIRECTOR ATTN AMSRL OP SD TP US ARMY RESEARCH LAB 2800 POWDER MILL RD ADELPHI MD 20783-1145
2	COMMANDER ATTN SMCAR TDC US ARMY ARDEC PCTNY ARSNL NJ 07806-5000
1	DIRECTOR ATTN SMCAR CCB TL BENET LABORATORIES ARSENAL STREET WATERVLIET NY 12189-4050
1	DIR USA ADVANCED SYSTEMS ATTN AMSAT R NR MS 219 1 R&A OFC AMES RESEARCH CENTER MOFFETT FLD CA 94035-1000

NO. OF COPIES	ORGANIZATION
1	COMMANDER ATTN AMSMI RD CS R DOC US ARMY MISSILE COMMAND REDSTONE ARSNL AL 35898-5010
1	COMMANDER ATTN AMSTA JSK ARMOR ENG BR US ARMY TANK AUTOMOTIVE CMD WARREN MI 48397-5000
1	DIRECTOR ATTN ATRC WSR USA TRADOC ANALYSIS CMD WSMR NM 88002-5502
1	COMMANDANT ATTN ATSH CD SECURITY MGR US ARMY INFANTRY SCHOOL FT BENNING GA 31905-5660

ABERDEEN PROVING GROUND

NO. OF COPIES	ORGANIZATION
2	DIR USAMSAA ATTN AMXSY D AMXSY MP H COHEN
1	CDR USATECOM ATTN AMSTE TC
1	DIR USAERDEC ATTN SCBRD RT
1	CDR USACBDCOM ATTN AMSCB CII
1	DIR USARL ATTN AMSRL SL I
5	DIR USARL ATTN AMSRL OP AP L

NO. OF COPIES	ORGANIZATION
1	HQDA (SARD-TR/MS. K. KOMINOS) WASH DC 20310-0103
1	HQDA (SARD-TR/DR. R. CHAIT) WASH DC 20310-0103
1	SDOP/TNI ATTN: L. H. CAVNEY PENTAGON WASHINGTON DC 20301-7100
6	COMMANDER, U.S. ARMY ARDEC ATTN: SMCAR-AET-A, R. DEKLEINE R. KLINE R. BOTTICELLI H. HUDGINS J. GRAU S. KAHN PICATINNY ARSENAL NJ 07806-5001
1	COMMANDER, U.S. ARMY ARDEC ATTN: SMCAR-CCH-V, PAUL VALENTI PICATINNY ARSENAL NJ 07806-5001
2	COMMANDER U.S. ARMY RESEARCH OFFICE ATTN: TECHNICAL LIBRARY D. MANN P.O. BOX 12211 RESEARCH TRIANGLE PARK NC 27709-2211
1	DIRECTOR U.S. ARMY RESEARCH OFFICE ATTN: AMXRO-MCS, MR. K. CLARK P.O. BOX 12211 RESEARCH TRIANGLE PARK NC 27709-2211
1	DIRECTOR U.S. ARMY RESEARCH OFFICE ATTN: AMXRO-RT-IP, LIBRARY SERVICES P.O. BOX 1211 RESEARCH TRIANGLE PARK NC 27709-2211
4	COMMANDER NAVAL RESEARCH LABORATORY ATTN: TECHNICAL LIBRARY CODE 4410, K. KAILASANATH J. BORIS E. ORAN WASHINGTON DC 20375-5000

NO. OF COPIES	ORGANIZATION
1	COMMANDER NAVAL SURFACE WARFARE CENTER ATTN: DR. F. MOORE DAHLGREN VA 22448
7	COMMANDER NAVAL SURFACE WARFARE CENTER ATTN: T. C. SMITH K. RICE S. MITCHELL S. PETERS J. CONSAGA C. GOTZMER TECHNICAL LIBRARY INDIAN HEAD MD 20640-5000
2	COMMANDER NAVAL SURFACE WARFARE CENTER ATTN: CODE R44, DR. A. WARDLAW K24, B402-12, DR. W. YANTA WHITE OAK LABORATORY SILVER SPRING MD 20903-5000
1	USAF WRIGHT AERONAUTICAL LABORATORIES ATTN: AFWAL/FIMG, DR. J. SHANG WPAFB OH 45433-6553
1	AFOSR/NA ATTN: J. TISHKOFF BOLLING AFB DC 20332-6448
3	AIR FORCE ARMAMENT LABORATORY ATTN: AFATL/FXA, STEPHEN C. KORN BRUCE SIMPSON DAVE BELK EGLIN AFB FL 32542-5434
2	WL/MNSH ATTN: R. DRABCZUK D. LITTRELL EGLIN AFB FL 32542-5434
1	LOS ALAMOS NATIONAL LABORATORY ATTN: MR. BILL HOGAN MS G770 LOS ALAMOS NM 87545

NO. OF COPIES	ORGANIZATION
2	DIRECTOR SANDIA NATIONAL LABORATORIES ATTN: DIV. 1554, DR. W. OBERKAMPF DIV. 1554, DR. F. BLOTTNER ALBUQUERQUE NM 87185
4	DIRECTOR NASA, LANGLEY RESEARCH CENTER ATTN: TECH LIBRARY MR. D. M. BUSHNELL DR. M. J. HEMSCH DR. J. SOUTH LANGLEY STATION HAMPTON VA 23665
2	DIRECTOR NASA, LANGLEY RESEARCH CENTER ATTN: MS 408, W. SCALLION D. WITCOFSKI HAMPTON VA 23605
6	DIRECTOR NASA, AMES RESEARCH CENTER ATTN: MS-227-8, L. SCHIFF MS-258-1, T. HOLST MS-258-1, D. CHAUSSEE MS-258-1, M. RAI MS-258-1, P. KUTLER MS-258-1, P. BUNING MOFFETT FIELD CA 94035
1	UNITED STATES MILITARY ACADEMY DEPARTMENT OF MECHANICS ATTN: LTC ANDREW L. DULL WEST POINT NY 10996
1	UNIVERSITY OF CALIFORNIA, DAVIS DEPT OF MECHANICAL ENGINEERING ATTN: PROF. H. A. DWYER DAVIS CA 95616
3	SCIENCE AND TECHNOLOGY INC. ATTN: DR. ALAN GLASSER MR. BRUCE LOHMAN MR. DAVE MAURIZI 4001 NORTH FAIRFAX DR., NO. 700 ARLINGTON VA 22203-1618

NO. OF COPIES	ORGANIZATION
1	MASSACHUSETTS INSTITUTE OF TECHNOLOGY ATTN: TECH LIBRARY 77 MASSACHUSETTS AVE. CAMBRIDGE MA 02139
1	GRUMANN AEROSPACE CORPORATION AEROPHYSICS RESEARCH DEPARTMENT ATTN: DR. R. E. MELNIK BETHPAGE NY 11714
1	AEDC CALSPAN FIELD SERVICE ATTN: MS 600, DR. JOHN BENEK TULLAHOMA TN 37389
1	VIRGINIA POLYTECHNIC INSTITUTE AND STATE UNIVERSITY DEPARTMENT OF AEROSPACE AND OCEAN ENGINEERING ATTN: DR. CLARK H. LEWIS BLACKSBURG VA 24061
1	ADVANCED TECHNOLOGY CENTER ARVIN/CALSPAN AERODYNAMICS RESEARCH DEPARTMENT ATTN: DR. M. S. HOLDEN P.O. BOX 400 BUFFALO NY 14225
1	THE PENNSYLVANIA STATE UNIVERSITY DEPT OF AEROSPACE ENGINEERING ATTN: DR. G. S. DULIKRAVICH UNIVERSITY PARK PA 16802
3	THE PENNSYLVANIA STATE UNIVERSITY DEPT OF MECHANICAL ENGINEERING ATTN: V. YANG K. KUO C. MERKLE UNIVERSITY PARK PA 16802-7501
1	UNIVERSITY OF ILLINOIS AT URBANA CHAMPAIGN DEPARTMENT OF MECHANICAL AND INDUSTRIAL ENGINEERING ATTN: DR. J. C. DUTTON URBANA IL 61801

NO. OF COPIES	ORGANIZATION
1	UNIVERSITY OF MARYLAND DEPT OF AEROSPACE ENGINEERING ATTN: DR. J. D. ANDERSON, JR. COLLEGE PARK MD 20742
1	UNIVERSITY OF NOTRE DAME DEPT OF AERONAUTICAL AND MECHANICAL ENGINEERING ATTN: PROF. T. J. MUELLER NOTRE DAME IN 46556
1	UNIVERSITY OF TEXAS DEPT OF AEROSPACE ENGINEERING MECHANICS ATTN: DR. D. S. DOLLING AUSTIN TX 78712-1055
1	UNIVERSITY OF DELAWARE DEPT OF MECHANICAL ENGINEERING ATTN: DR. JOHN MEAKIN, CHAIRMAN NEWARK DE 19716
1	ARROW TECHNOLOGY ASSOCIATES, INC. ATTN: W. HATHAWAY P.O. BOX 4218 SOUTH BURLINGTON VT 05401-0042
1	PAUL GOUGH ASSOCIATES, INC. ATTN: P. S. GOUGH 1048 SOUTH ST. PORTSMOUTH NH 03801-5423
2	PRINCETON COMBUSTION RESEARCH LABORATORIES, INC. ATTN: N. MER N. A. MESSINA PRINCETON CORPORATE PLAZA 11 DEERPARK DR., BLDG. IV, SUITE 119 MONMOUTH JUNCTION NJ 08852
1	ROCKWELL INTERNATIONAL ROCKETDYNE DIVISION ATTN: BA08, R. B. EDELMAN 6633 CANOGA AVE. CANOGA PARK CA 91303-2703
2	ROCKWELL INTERNATIONAL SCIENCE CENTER ATTN: DR. S. CHAKRAVARTHY DR. S. PALANISWAMY 1049 CAMINO DOS RIOS THOUSAND OAKS CA 91360

NO. OF COPIES	ORGANIZATION
1	VERITAY TECHNOLOGY, INC. ATTN: E. FISHER 4845 MILLERSPORT HIGHWAY EAST AMHERST NY 14501-0305
	ABERDEEN PROVING GROUND
31	DIR, USARL ATTN: AMSRL-WT-P, MR. ALBERT HORST AMSRL-WT-PB, DR. E. SCHMIDT MR. B. GUIDOS DR. P. PLOSTINS DR. J. SAHU MR. P. WEINACHT DR. G. COOPER AMSRL-WT, DR. A. BARROWS AMSRL-WT-PD, DR. B. BURNS AMSRL-WT-PA, DR. T. MINOR MR. M. NUSCA (7 CP) MS. G. WREN DR. T. COFFEE MR. J. DESPIRITO DR. D. KOOKER MR. D. KRUCZYNSKI DR. G. KELLER DR. F. LIBERATORE AMSRL-WT-W, DR. C. MURPHY AMSRL-WT-WB, DR. W. D'AMICO AMSRL-WT-NC, MS. D. HISLEY MR. R. LOTTERO DR. K. OPALKA AMSRL-CI-C, DR. W. STUREK DR. N. PATEL
3	DIR USAERDEC ATTN SCBRD-RTB, MR. D. PALUGHI MR. L. BICKFORD DR. S. THOMPSON

USER EVALUATION SHEET/CHANGE OF ADDRESS

This Laboratory undertakes a continuing effort to improve the quality of the reports it publishes. Your comments/answers to the items/questions below will aid us in our efforts.

1. ARL Report Number ARL-TR-663 Date of Report January 1995

2. Date Report Received ____________________

3. Does this report satisfy a need? (Comment on purpose, related project, or other area of interest for which the report will be used.) ____________________

4. Specifically, how is the report being used? (Information source, design data, procedure, source of ideas, etc.) ____________________

5. Has the information in this report led to any quantitative savings as far as man-hours or dollars saved, operating costs avoided, or efficiencies achieved, etc? If so, please elaborate. ____________________

6. General Comments. What do you think should be changed to improve future reports? (Indicate changes to organization, technical content, format, etc.) ____________________

CURRENT ADDRESS

Organization

Name

Street or P.O. Box No.

City, State, Zip Code

7. If indicating a Change of Address or Address Correction, please provide the Current or Correct address above and the Old or Incorrect address below.

OLD ADDRESS

Organization

Name

Street or P.O. Box No.

City, State, Zip Code

(Remove this sheet, fold as indicated, tape closed, and mail.)

(DO NOT STAPLE)

DEPARTMENT OF THE ARMY

OFFICIAL BUSINESS

NO POSTAGE
NECESSARY
IF MAILED
IN THE
UNITED STATES

BUSINESS REPLY MAIL
FIRST CLASS PERMIT NO 0001, APG, MD

Postage will be paid by addressee

Director
U.S. Army Research Laboratory
ATTN: AMSRL-OP-AP-L
Aberdeen Proving Ground, MD 21005-5066